ARTICLES

Stability of Silver Nanoparticles Fabricated by Nanosphere Lithography and Atomic Layer Deposition to Femtosecond Laser Excitation

Jiha Sung,[†] Kathryn M. Kosuda,[†] Jing Zhao,[†] Jeffrey W. Elam,[‡] Kenneth G. Spears,[†] and Richard P. Van Duyne*,[†]

Department of Chemistry, Northwestern University, Evanston, Illinois 60208-3113 and Chemistry Division and Energy Systems Division, Argonne National Laboratory, 9700 South Cass Avenue, Argonne, Illinois 60439

Received: September 14, 2007; In Final Form: January 17, 2008

In this paper, we compare the stability of silver nanoparticles fabricated by nanosphere lithography (NSL) and those coated with atomic layers of Al_2O_3 to femtosecond laser pulses. Structural changes in the nanoparticles caused by the laser pulses were monitored by UV−vis extinction spectroscopy. It is demonstrated that 1.0 nm thick Al_2O_3 layers fabricated by atomic layer deposition (ALD) provide a factor of 10 improvement in the stability of the silver nanoparticles against femtosecond laser exposure compared to that for bare nanoparticles. The enhanced stability caused by the Al_2O_3 layers is explained by the increased surface melting temperature resulting from the decreased mean square displacement of silver atoms located on the nanoparticle surface. This study demonstrates that Al_2O_3-coated nanoparticles can serve as a stable platform for both linear and nonlinear ultrafast surface-enhanced laser spectroscopy.

I. Introduction

Noble metal nanoparticles have optical properties that are different from those of the bulk. These properties originate from the localized surface plasmon resonance (LSPR), which is a collective oscillation of the conduction electrons that occurs when light impinges on a nanoparticle at a specific wavelength. The remarkable consequences of this optical phenomenon are enhanced light scattering and absorption and large local field enhancement near the nanoparticle surface at the resonant condition. The LSPR can be controlled by changing the size, shape, and composition of the nanoparticle[1−3] as well as the dielectric environment.[4,5] These features of LSPR have enabled noble metal nanoparticles to be applied for a variety of applications, including bio/chemosensors,[6−9] optical filters,[10,11] plasmonic waveguides,[12−15] and surface-enhanced spectroscopy.[16−18]

Surface-enhanced Raman scattering (SERS) is one of the most studied surface-enhanced spectroscopic techniques to date.[17,19−21] Local field enhancements by the LSPR have been determined as the origin of the huge enhancement of Raman scattering from molecules adsorbed on noble metal nanoparticles or nanostructures. Recently, surface-enhanced nonlinear spectroscopic studies of molecules adsorbed on noble metal nanoparticles or nanostructures have also been reported, including second-harmonic generation,[22−24] sum frequency generation,[25−27] coherent anti-Stokes Raman scattering,[28−31] hyper-Raman scattering,[32] and two-photon absorption.[33]

Noble metal nanoparticles or nanostructures have been shown to be excellent substrates for surface-enhanced laser spectroscopy, and it is important to characterize the interaction between a laser pulse and the metal nanoparticles. There have been studies to explore the relaxation dynamics of noble metal nanoparticles that are excited by femtosecond laser pulses. Electron−electron, electron−phonon, and phonon−phonon relaxation in gold and silver nanoparticles with various sizes and shapes have been studied by time-resolved pump−probe spectroscopy.[34] Coherent vibrational oscillation of noble metal nanoparticles induced by femtosecond excitation also has been monitored by pump−probe transient spectroscopy. The Hartland group and the El-Sayed group monitored the transient absorption signal versus the delay time of the probe beam for colloidal gold nanoparticles[35−37] and gold and silver nanoparticle arrays fabricated by nanosphere lithography (NSL).[38] They monitored the oscillation of transient absorption signals with various probe beam wavelengths and found that oscillations on the blue and the red side of the extinction maximum wavelength of the nanoparticle showed a 180° phase difference. El-Sayed and coworkers also discussed the effect of interparticle coupling on the period of lattice oscillation in the case of NSL-fabricated gold and silver nanoparticle arrays.[39]

For nonlinear laser spectroscopies, high laser intensity is often required to obtain a reasonable signal level. However, metal nanoparticles are susceptible to melting or deformation[40−42] by the heat induced through the relaxation process of hot electrons excited by the high-power ultrashort laser pulses that are used for nonlinear spectroscopic techniques. Furthermore, the lowered melting temperature of the nanoparticles compared to that of the bulk metal can accelerate the melting and deformation of the nanoparticles.[43−48]

* To whom correspondence should be addressed. E-mail: vanduyne@northwestern.edu.
[†] Northwestern University.
[‡] Argonne National Laboratory.

10.1021/jp0774140 CCC: $40.75
Published on Web 03/25/2008

Recently, Van Duyne and co-workers[49] demonstrated that the Al_2O_3 film deposited on silver nanoparticle arrays by atomic layer deposition (ALD) can protect the nanoparticles from thermal deformation. They suggested the possibility of using Al_2O_3-coated silver nanoparticles as a substrate for operando SERS studies which require high temperatures and pressures employed in industrial catalytic reactions.[49,50] In this work, we present studies on the femtosecond laser power stability of NSL-fabricated silver nanoparticles on glass substrates. Bare silver nanoparticles and nanoparticles coated with a thin Al_2O_3 film deposited by ALD were irradiated by a femtosecond laser, and their LSPR shift was monitored by white light extinction measurements. The laser wavelengths were either resonant or off-resonant to the LSPR of the silver nanoparticles. Al_2O_3-coated silver nanoparticles showed enhanced stability against the laser exposure, and it is proposed that Al_2O_3-coated nanoparticles can be used as a stable platform for both linear and nonlinear surface-enhanced laser spectroscopy.

II. Experimental Methods

A. Materials. Silver pellets (99.99%) were purchased from the Kurt J. Lesker Company (Pittsburgh, PA). Glass substrates (no. 2, 18 mm diameter cover slips) were purchased from Fisher Scientific (Hampton, NH). Surfactant-free, white carboxyl-substituted polystyrene latex nanospheres with diameter (D) = 390 nm were received as a suspension in water from Duke Scientific (Palo Alto, CA). Absolute ethanol was purchased from Pharmco (Brookfield, CT). Trimethylaluminum (TMA) for the fabrication of Al_2O_3 atomic layers was purchased from Sigma Aldrich (Milwaukee, WI).

B. Preparation of Silver Nanoparticle Samples. Glass substrates were cleaned by immersion in a boiling piranha solution (3:1 concentrated H_2SO_4/30% H_2O_2) for 30 min. (CAUTION: *Piranha reacts violently with organic compounds and should be handled with great care.*) After cooling, the substrates were thoroughly rinsed repeatedly with 18.2 MΩ cm^{-1} Millipore water (Marlborough, MA). The substrates were then sonicated for 1 h in 5:1:1 H_2O/NH_4OH/30% H_2O_2. Following sonication, the substrates were rinsed with copious amounts of Millipore water.

Single-layer, monodispersed silver nanoparticles were prepared with the NSL technique.[2,51] A suspension of nanospheres spontaneously self-assembled into hexagonally close-packed two-dimensional arrays after being coated on a clean glass substrate. Silver was deposited at a rate of 0.1 nm s^{-1} with a Kurt J. Lesker Axxis electron beam deposition system (Pittsburgh, PA) with a base pressure of 10^{-6} Torr. The deposited height (d_m) was monitored with a Sigma Instruments 6 MHz gold-plated quartz crystal microbalance (Fort Collins, CO). The nanosphere masks were removed from the substrate by sonication in absolute ethanol for approximately 5 min.

Al_2O_3 films were grown by ALD on silver nanoparticles fabricated by NSL. The reactor utilized in these experiments is similar to one described in previous publications.[52] Trimethylaluminum (TMA) and deionized H_2O vapors were alternately dosed over the substrates in a nitrogen carrier stream at a mass flow rate of 360 sccm and a pressure of ~1 Torr, using a growth temperature of 50 °C. Al_2O_3 ALD proceeded according to the following pair of self-limiting reactions, where the asterisks (*) denote the surface species:[53]

$$Al{-}OH^* + Al(CH_3)_3 \rightarrow Al{-}O{-}Al(CH_3)_2^* + CH_4 \quad (A)$$

$$Al{-}CH_3^* + H_2O \rightarrow Al{-}OH^* + CH_4 \quad (B)$$

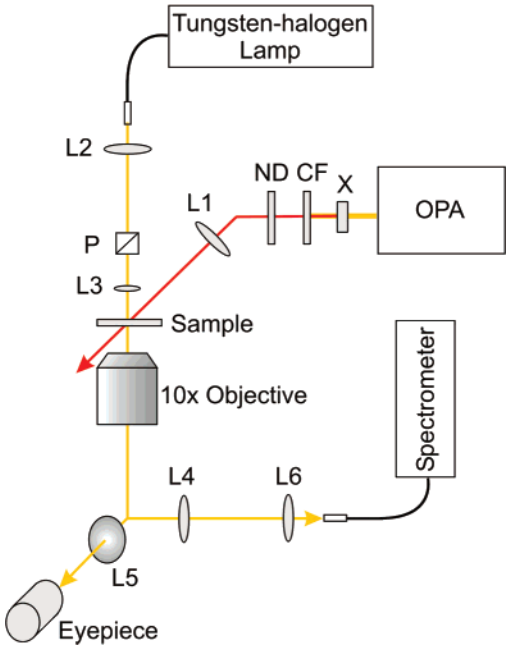

Figure 1. Experimental apparatus used for laser irradiation and extinction measurements. Symbols represent L1: +80 mm CaF_2 lens; L2: +40 mm achromatic lens; L3: +12.7 mm achromatic lens; L4 and L5: +200 mm achromatic lens (tube lens); L6: +30 mm achromatic lens; P: Glan-Taylor calcite polarizer; X: 0.6 mm type-I BBO crystal; CF: short-pass color filter; and ND: round continuously variable neutral density filter.

One complete ALD cycle consists of four steps: (1) TMA reactant exposure time, 2 s; (2) N_2 purge following TMA exposure, 10 s; (3) H_2O reactant exposure time, 2.5 s; (4) N_2 purge following H_2O exposure, 30 s. Long purge times are necessary at low temperatures to prevent chemical vapor deposition of Al_2O_3.[54] In a previous study, Al_2O_3 growth on silver surfaces by ALD was shown to proceed with an average growth rate of ~1 Å/cycle.[55]

For our experiments, NSL-fabricated silver nanoparticles were exposed to 4 or 10 ALD cycles, corresponding to an Al_2O_3 thickness of 0.4 or 1.0 nm, respectively.

C. Measurement of the Stability of Silver Nanoparticles upon Laser Exposure. Experiments were carried out with an amplified Ti:Sapphire laser system described in prior publications.[56,57] The output of the compressor is centered at 805 nm, with a spectral bandwidth of 22 nm and pulse duration of 90 fs at 1 kHz. A tunable near-IR fundamental beam was generated with a laboratory-built optical parametric amplifier (OPA) pumped by 650 μJ/pulse of the amplified Ti:Sapphire laser beam. The total near-IR output of the OPA was 50 μJ/pulse (signal + idler). A polarizer separated the signal and idler pulses. The duration and bandwidth of the signal pulse are 125 fs and 430 cm^{-1} (at 1.3 μm), respectively.

The laser irradiation on the sample and the extinction measurements were performed using a laboratory-built microscope setup. Figure 1 shows the schematic diagram of the setup. The variable signal output of the OPA (tunable range of 1.16−1.52 μm) was doubled by a 0.6 mm thickness type-I β-barium borate (BBO) crystal, and the fundamental near-IR beam was blocked by a short-pass color filter (Schott KG-3). The resulting visible beam was focused onto the sample by a +80 mm focal length CaF_2 lens with a 45° incidence angle. Two different laser wavelengths were used for the laser power stability measurements of NSL-fabricated silver nanoparticles. One was the wavelength that corresponds to the LSPR extinction maximum

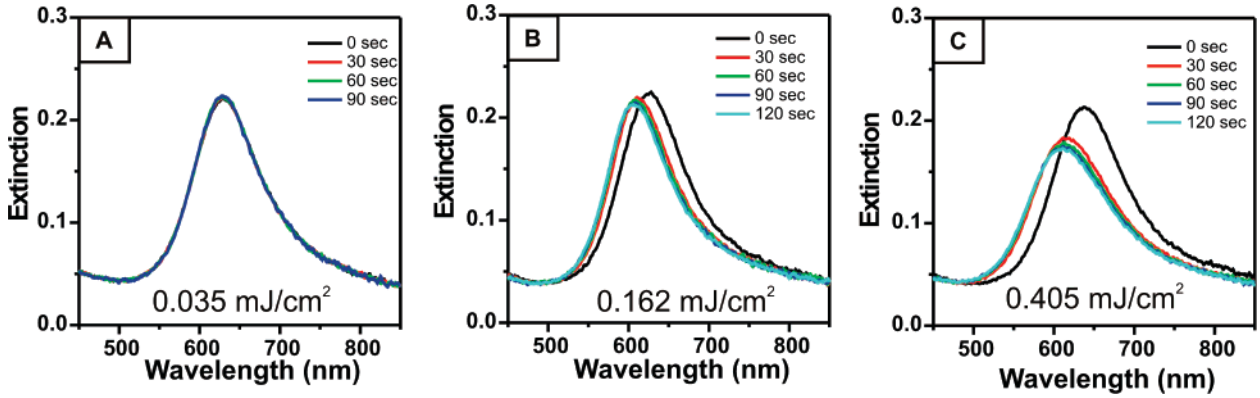

Figure 2. LSPR change after laser exposure to the bare silver nanoparticles ($D = 390$ nm, $d_m = 30$ nm). The wavelength of the incident laser was 630 nm. The laser pulse intensity was (A) 0.035 (B) 0.162, and (C) 0.405 mJ cm^{-2}.

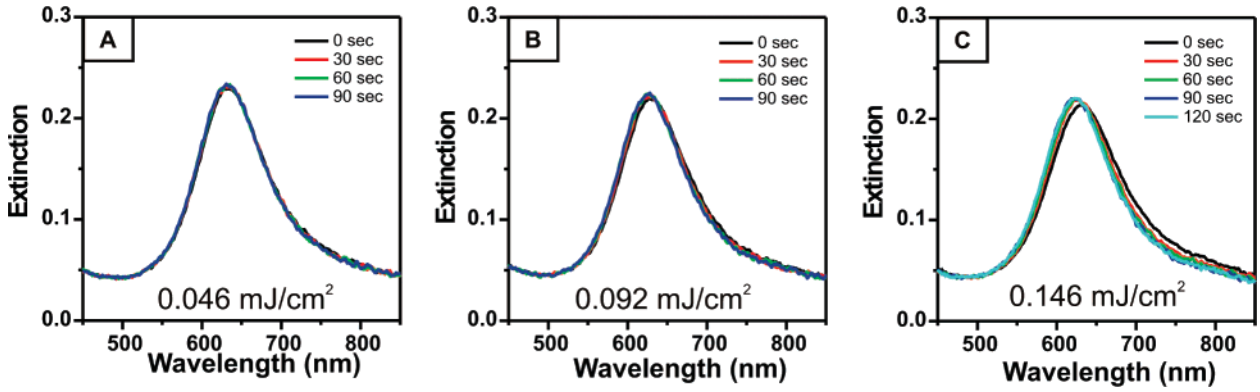

Figure 3. LSPR change after laser exposure to the bare silver nanoparticles ($D = 390$ nm, $d_m = 30$ nm). The wavelength of the incident laser was 730 nm. The laser pulse intensity was (A) 0.046, (B) 0.092, and (C) 0.146 mJ cm^{-2}.

(LSPR λ_{max}) of the nanoparticles, which will be called the resonant condition. The other was a wavelength that was ~100 nm red-shifted from the LSPR λ_{max} and will be called the off-resonant condition. The laser wavelengths tested were 630 and 730 nm for bare nanoparticles and 610 and 710 nm for nanoparticles coated with 0.4 and 1.0 nm of Al_2O_3. The spot size of the beam at the focus was scanned with a straight edge and was close to Gaussian, with 25.2 μm full width at half-maximum (fwhm) along the long axis. The beam intensity was controlled with a round continuously variable neutral density filter.

Extinction spectra were measured with an Ocean Optics USB2000 fiber-coupled spectrometer. White light from a tungsten−halogen lamp was fiber-coupled with a 100 μm fiber to a +40 mm focal length achromatic collimating lens. The collimated beam was then polarized by a Glan-Taylor calcite polarizer with a 5 mm aperture and focused onto the sample by a +12.7 mm focal length achromatic lens with the optic axis normal to the sample surface. The beam was carefully aligned to monitor the spot of laser focus. The diameter of the white light spot on the sample was 20 μm at fwhm. Transmitted light was collected by an infinity-corrected 10× Nikon microscope objective (NA = 0.30) at a working distance of 16.0 mm and directed to the spectrometer or an eyepiece by the choice of the mirror mounted after the objective. When the extinction was measured, the beam was focused into a 600 μm fiber that couples into the spectrometer.

The extinction of NSL-fabricated silver nanoparticles was monitored during the femtosecond laser irradiation. The extinction spectra were obtained before laser irradiation and at 30 s intervals of laser exposure. While the extinction spectra were recorded, the laser beam was blocked in order to prevent the scattered laser light from entering the spectrometer.

III. Results and Discussion

A. Laser Induced LSPR Change of the Bare Silver Nanoparticles. The LSPR of NSL-fabricated silver nanoparticles is very sensitive to the particle size and tip sharpness.[2,58] For the NSL-fabricated silver nanoparticles, a blue shift of the LSPR wavelength maximum (LSPR λ_{max}) has been observed when the tip of the nanoparticle is rounded by a solvent,[58] heat,[49,59] or electrochemical oxidation.[60] Theory also predicts a blue shift of the LSPR λ_{max} when comparing triangular nanoprisms with blunt versus sharp tips.[5] Therefore, any shape change in the nanoparticles from the laser irradiation can be monitored by the LSPR band shift.

Figure 2 shows the LSPR spectra of bare silver nanoparticles before and after laser exposure with different laser pulse intensities and exposure times. The NSL-fabricated nanoparticles with $D = 390$ nm and $d_m = 30$ nm have an LSPR λ_{max} at ~630 nm, and the wavelength of the laser was tuned to 630 nm. After laser exposure, the LSPR blue-shifted. The same measurements with the 730 nm wavelength laser beam, which is about 100 nm off-resonant from the LSPR λ_{max}, are shown in Figure 3. Again, a blue shift of the LSPR after laser exposure was observed. The LSPR shift versus laser exposure time is plotted in Figure 4. For both the resonant and off-resonant conditions, the majority of the shift is observed with the first 30 s laser exposure, and then, the LSPR shift gradually saturates. The LSPR shift increases as the laser pulse intensity increases. The laser pulse intensity was calculated from the area within the radius of the standard deviation of the Gaussian laser intensity profile. The standard deviation was 10.7 μm for the long axis

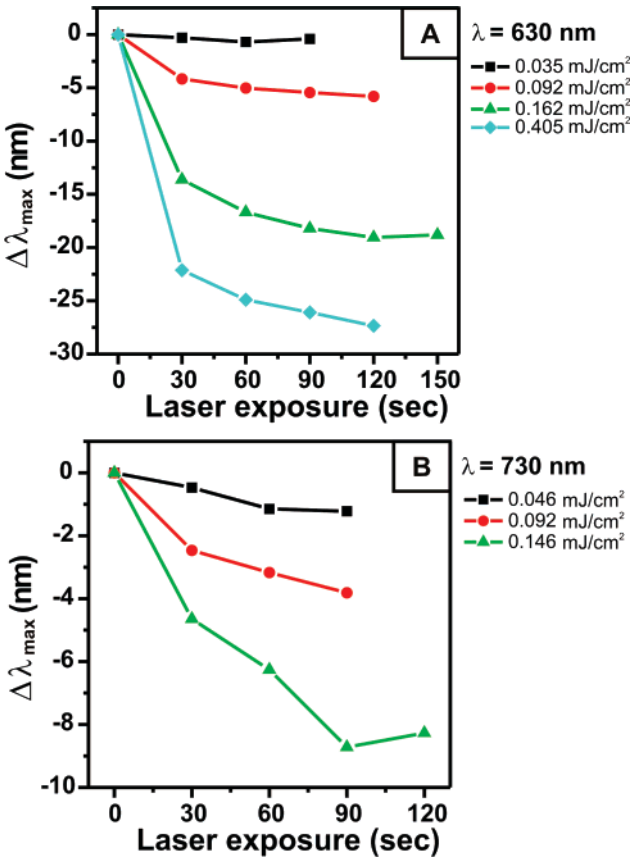

Figure 4. LSPR shift versus laser exposure time for bare nanoparticles (D = 390 nm, d_m = 30 nm). The wavelength of the incident laser was (A) 630 and (B) 730 nm.

of the beam spot, and 68% of the total beam intensity was focused in the area.

The reshaping of NSL-fabricated gold nanoparticles by a femtosecond laser pulse has been reported by El-Sayed and co-workers.[47,48] They excited gold nanoparticles with a 400, 800, and 700 nm laser that corresponded to the interband/in-plane quadrupolar transition, dipolar transition, and both quadrupolar and dipolar transition, respectively. The LSPR and shape change of the gold nanoparticles were monitored by extinction spectra measurement and scanning electron microscopy (SEM). When the dipolar transition was excited, which is the case for our experiments, a blue shift of the LSPR band was observed, which agrees with our results, despite differences in detailed spectral features. El-Sayed and co-workers observed rounding of the tips for gold nanoparticles exposed to a 3.0 mJ cm^{-2} laser pulse and the displacement or removal of nanoparticles from the substrate with pulse intensities greater than 5.0 mJ cm^{-2}.[47,48] The rounded tips were explained by photothermal heating, and the displacement of the nanoparticles with high power laser irradiation was explained by gold atom sublimation, which causes a rapid buildup of pressure underneath the particle and propels it from the surface.[47,48,61] In our experiments, laser pulse intensities were lower than 1 mJ cm^{-2}, and therefore, displacement or removal of nanoparticles is not expected.

When the conduction electrons in noble metal nanoparticles are excited by a femtosecond laser pulse, excited electrons undergo relaxation processes through electron−electron, electron−phonon, and phonon−phonon coupling.[34] Through the electron−phonon coupling, the energy is exchanged between the electrons and the lattice,[34] which results in lattice heating. The heat is dissipated through the phonon−phonon coupling between the nanoparticles and the surrounding media. The time constant of the electron−electron relaxation is on the order of several hundred femtoseconds[62,63] and the electron−phonon relaxation is on the order of several picoseconds,[64] which has a particle size dependence.[65] The phonon−phonon relaxation is on the order of several hundred picoseconds,[34,66,67] revealing that the heat conductivity of the surrounding media is an important factor. In our experiment, the glass substrate serves as an energy sink. Once the nanoparticles are excited by a femtosecond pulse, all of the relaxation processes are completed before the next laser pulse excites the nanoparticles again since all of the relaxation processes are faster than the 1 kHz laser repetition rate that was used for our experiment. Therefore, we can estimate the temperature of the silver nanoparticles right after exposure to the laser pulse.

In the case of exposure to the 630 nm wavelength laser pulse, the energy absorbed by each nanoparticle is approximately 6.83 $\times$ 10^{-15}, 3.15 $\times$ 10^{-14}, and 7.88 $\times$ 10^{-14} J for a laser pulse intensity of 0.035, 0.162, and 0.405 mJ cm^{-2}, respectively. The extinction of silver nanoparticles at 630 nm is approximated to be 0.2 (transmittance = 0.63). To estimate the contribution of absorption to extinction, an electrodynamics calculation using the discrete dipole approximation method[5,68] was performed on a silver nanoparticle with similar shape and size. From the calculation, the contributions of absorption and scattering to extinction are about 80 and 20% at the resonant wavelength, respectively. The calculated temperatures of the silver nanoparticle based on energy absorbed are 308, 364, and 467 K, respectively. The heat capacity of silver is estimated to be 25.35 J M^{-1} K^{-1}, its value at 298.15 K. This estimation is reasonable since the heat capacity of silver varies by less than 7% until 600 K.[69] The melting temperature of bulk silver is 1234.93 K. However the nanoparticle shows a large depression in melting temperature with decreasing size, or radius, which is caused by the high surface tension of the nanoparticle.[44,45,70] Even though the melting temperature of our nanoparticle is close to that of the bulk, because of the large curvature at the tip area, the sharp tips can have a melting point low enough to be melted by the energy provided by the laser pulse. NSL silver nanoparticles fabricated using a sphere diameter of less than 264 nm have been reported to undergo surface melting even at room temperature.[71] The rounded tip results in a blue shift of the LSPR band of the silver nanoparticles. SEM images were obtained for the nanoparticles with and without laser exposure, but no differences were observed within our resolution (data not shown). The LSPR of the nanoparticle array is very sensitive to changes in tip geometry, and therefore, even a slight tip rounding that cannot be detected by SEM can cause an LSPR λ_{max} shift of ~25 nm, which was the maximum shift observed with our laser intensities.

In the case of exposure to the 730 nm wavelength laser pulse, the energy absorbed by a single nanoparticle was less than in the case of the 630 nm pulse because it corresponds to the tail of the LSPR band where the absorption is smaller. Therefore, tip melting is not efficient at this condition, which leads to a smaller blue shift than the 630 nm laser pulse with similar energy would produce.

B. Laser-Induced LSPR Change of ALD Al_2O_3-Coated Nanoparticles. The LSPR changes induced by the laser pulse were monitored for silver nanoparticles fabricated by NSL (D = 390 nm and d_m = 50 nm) and coated with 0.4 and 1.0 nm of ALD Al_2O_3. The LSPR λ_{max} of both samples was ~610 nm, and the wavelength of the laser was tuned to 610 and 710 nm to test the laser power stability of the samples for the resonant

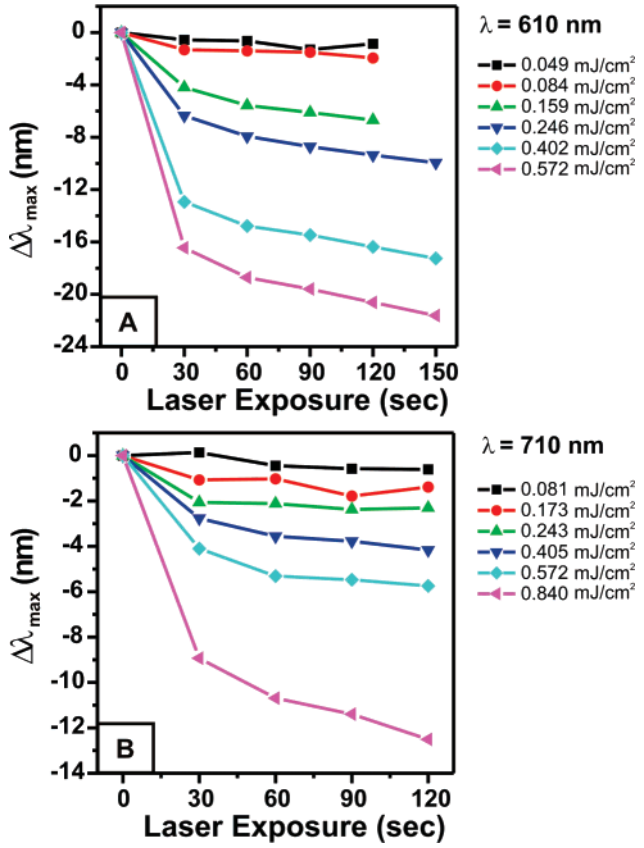

Figure 5. LSPR shift versus laser exposure time for nanoparticles (D = 390 nm, d_m = 50 nm) coated with 0.4 nm of Al_2O_3. The wavelength of the incident laser was (A) 610 and (B) 710 nm.

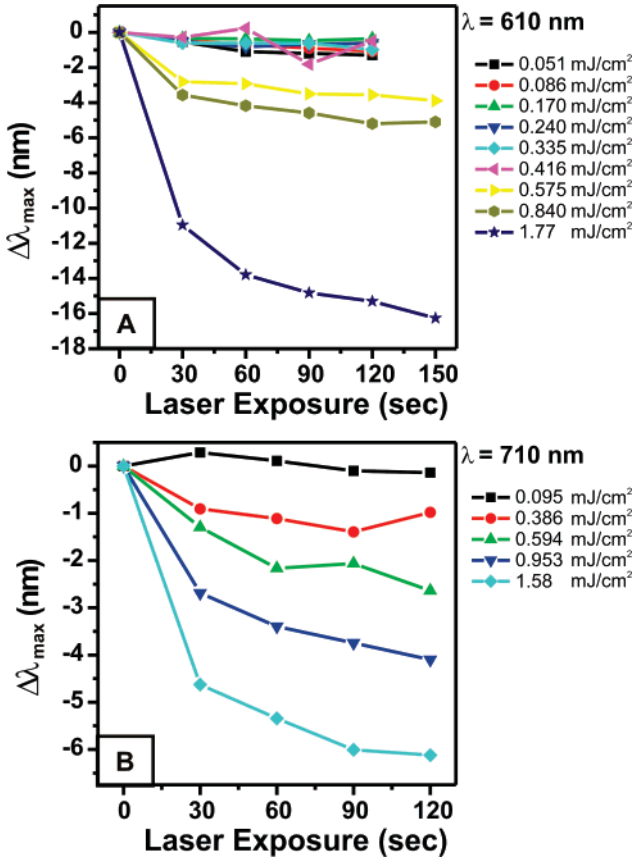

Figure 6. LSPR shift versus laser exposure time for nanoparticles (D = 390 nm, d_m = 50 nm) coated with 1.0 nm of Al_2O_3. The wavelength of the incident laser was (A) 610 and (B) 710 nm.

and off-resonant conditions. Figures 5 and 6 show the LSPR shift versus laser exposure time for nanoparticles coated with 0.4 and 1.0 nm of Al_2O_3, respectively. For both the resonant and off-resonant conditions, the majority of shift is observed with the first 30 s laser exposure, followed by a gradual saturation of the LSPR shift. This is similar to what was observed for the bare nanoparticles. A larger LSPR shift is observed with the 610 nm laser wavelength as compared to the 710 nm laser wavelength with similar pulse intensities. Larger shifts in the resonant condition were also seen for the bare nanoparticles. However, the absolute amount of the LSPR shift of the bare nanoparticles, nanoparticles with 0.4 nm of Al_2O_3, and nanoparticles with 1.0 nm of Al_2O_3 for similar laser pulse intensities varies with respect to each other. Figure 7 shows the LSPR shift of bare nanoparticles (black squares) and nanoparticles with 0.4 (red circles) and 1.0 nm of Al_2O_3 (green triangles) after 120 s of laser exposure versus laser pulse intensity. The resonant condition is plotted with solid marks, and the off-resonant condition is plotted with open marks. All of the plots show an increase in the LSPR shift as the laser pulse intensity increases. For the same laser pulse intensity, the bare nanoparticles undergo the largest LSPR shift, and the nanoparticles with 1.0 nm of Al_2O_3 show the smallest shift against the laser exposure. The laser pulse energy of 1.77 mJ cm^{-2} that led to an LSPR shift of ~15 nm for the sample with 1.0 nm of Al_2O_3 in resonant condition can heat the nanoparticles up to 748 K. The LSPR shift is similar to the shift in bare nanoparticles induced by the pulse energy of 0.162 mJ cm^{-2}, which can heat the nanoparticles only up to 422 K.

The LSPR λ_{max} shift shows an approximately linear relation to the laser pulse intensity within our intensity range. In the

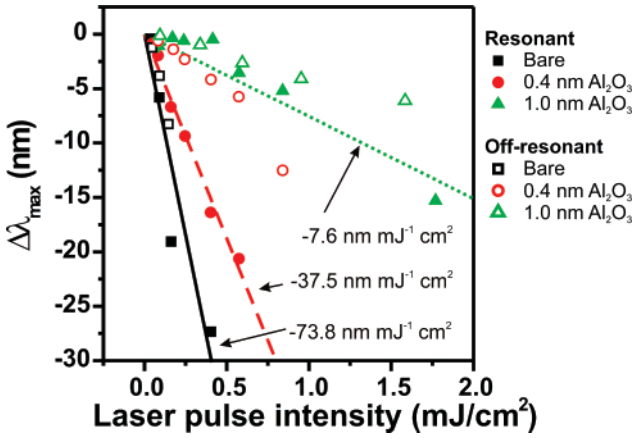

Figure 7. LSPR shift after 120 s of laser exposure versus laser pulse intensity. The resonant condition is plotted with solid marks, and the off-resonant condition is plotted with open marks. Linear fitting for the resonant condition is shown with solid black line, red dashed line, and green dotted line for bare particles, nanoparticles coated with 0.4 nm of Al_2O_3, and nanoparticles coated with 1.0 nm of Al_2O_3, respectively. Slopes for each sample are −73.8, −37.5, and −7.6 nm mJ^{-1} cm^2 for resonant condition and −50.8, −12.6, and −4.0 nm mJ^{-1} cm^2 for off-resonant condition.

case of the resonant condition, the slopes are −73.8, −37.5, and −7.6 nm mJ^{-1} cm^2 for bare nanoparticles, nanoparticles with 0.4 nm of Al_2O_3, and nanoparticles with 1.0 nm of Al_2O_3, respectively, as shown in Figure 7. This means that if the nanoparticles coated with 1.0 nm of Al_2O_3 are used as a substrate for laser spectroscopy, 10 times higher laser pulse intensity can be used compared to that when the bare nanoparticles are used

as substrates. In the case of the off-resonant condition, the slopes are −50.8, −12.6, and −4.0 nm mJ^{-1} cm^2, respectively.

As a mechanism of the protection from the laser deformation of Al_2O_3-coated silver nanoparticles, it might be suggested that the Al_2O_3 layers serve as an additional heat sink. In such a case, suppression of the surface melting by the Al_2O_3 layers can be explained by the increased electron−phonon and phonon−phonon relaxation time, which leads to the efficient cooling of the hot nanoparticles. Also, it has been reported that molecules adsorbed on gold nanoshells can introduce an additional hot electron decay channel, which leads to a decreased relaxation time.[72] However, Whitney et al. reported that Al_2O_3 layers protect the silver nanoparticles from thermally induced deformation at the thermal equilibrium condition.[49] They compared the LSPR shift of bare silver nanoparticles and nanoparticles coated with Al_2O_3 after heating at 100−500 °C for several hours and observed that the Al_2O_3-coated nanoparticles showed greatly reduced LSPR shifts compared to those of the bare nanoparticles.[49] This was also verified by SEM imaging.[49] Their work implies that the increased relaxation rate is not the major factor in the protection of the silver nanoparticles from the laser-induced surface melting for Al_2O_3-coated nanoparticles.

The surface melting in nanocrystals has been discussed by Shi[44] using the Lindemann criterion.[73] According to the Lindemann criterion, a crystal melts when the root-mean-square displacement of the atoms in the crystal exceeds a certain fraction of the interatomic distance.[44] The melting temperature for a nanocrystal is given by[44]

$$\frac{T}{T_0} = \exp[-(\alpha - 1)n_s/n_v] \quad (1)$$

where T is the melting temperature of the nanocrystal, T_0 is the melting temperature of the bulk, and n_s and n_v are the number of surface atoms and the number of atoms located within the particle volume, respectively. The ratio n_s/n_v implies the particle size (or curvature) dependence of the melting temperature. As the particle size reduces, n_s/n_v increases. The α is given by σ_s/σ_v, where σ_s and σ_v are mean square displacements of the atoms located on the surface and within the particle, respectively. In most cases, $\sigma_s > \sigma_v$, that is, $\alpha > 1$ because surface atoms are loosely bound compared to the bulk atoms. Therefore, as the particle size decreases and n_s/n_v increases, T decreases. As α approaches the value of 1, the particle size sensitivity of the melting temperature decreases, and the melting temperature of the nanoparticle approaches that of the bulk. In the case of the silver nanoparticles coated with Al_2O_3, the Al_2O_3 layers serve as a rigid frame for the silver nanoparticles and suppress the thermal vibration of the surface atoms of the nanoparticles. As a result, σ_s, and therefore α, of the Al_2O_3-coated nanoparticles decreases compared to that of bare nanoparticles, which leads to the increased melting temperature of the Al_2O_3-coated nanoparticles compared to that of the bare nanoparticles. This model provides a clear explanation for how the Al_2O_3 layers protect the silver nanoparticles from surface melting.

The saturation behavior of the LSPR shift versus laser exposure observed in Figures 4−6 is a result of two effects. First, as the LSPR extinction maximum shifts to bluer wavelengths, the incident laser is less efficiently absorbed so that less energy is deposited in the nanoparticles. Second, we hypothesize that this behavior is also a consequence of the increased melting temperature of the nanoparticles. As the radius of curvature of the particle tip decreases with increased laser exposure, the ratio n_s/n_v in eq 1 decreases, which results in an increased melting temperature. Consequently, the $\Delta\lambda_{max}$ versus laser exposure time plots saturate after sufficient laser exposure time.

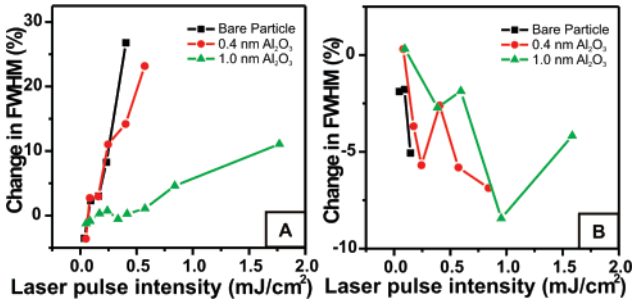

Figure 8. Percent change in the LSPR bandwidth after 120 s of laser exposure versus laser pulse intensity; (A) resonant condition and (B) off-resonant condition.

C. Change in LSPR Bandwidth after the Laser Exposure. After laser exposure, in addition to the LSPR shift, a corresponding change in the LSPR bandwidth was observed. For both the resonant and off-resonant conditions, the LSPR λ_{max} blue-shifted after laser exposure. However, the LSPR bandwidth increased for the resonant condition, and it decreased for the off-resonant condition, which is shown in Figures 2C and 3C.

In Figure 8, the percent change in the LSPR bandwidth after 120 s of laser exposure is plotted versus laser pulse energy for the (A) resonant condition and (B) off-resonant condition. The percent change is defined as the following

$$\text{percent change} = \frac{w_0 - w_L}{w_0} \times 100\ (\%) \quad (2)$$

where w_0 is the fwhm of the LSPR band before laser exposure and w_L is the fwhm after the 120 s laser exposure. Both bandwidths are measured in energy units. As shown in Figure 8A, when the laser wavelength was close to the LSPR λ_{max} and the laser pulse intensity was larger than 0.09 mJ cm^{-2}, the LSPR bandwidth increased. However, a slight decrease in bandwidth was observed when the laser pulse intensity was less than 0.09 mJ cm^{-2} for both bare and Al_2O_3-coated nanoparticles. The percent change increased as the laser pulse intensity increased. The percent change in the LSPR bandwidth when the laser wavelength was 100 nm apart from the LSPR λ_{max} is plotted in Figure 8B. The LSPR bandwidth was slightly decreased after laser exposure.

About 5000 silver nanoparticles are within the region that is probed by the white light. The nanoparticle size shows a Gaussian distribution, and its standard deviation is expected to be similar to the size distribution of the nanoparticles (standard deviation ∼ 5 nm) that are used for NSL.[71] When the wavelength of the laser is longer than the LSPR λ_{max} by 100 nm (off-resonant condition), the nanoparticles cannot be heated efficiently by the laser, but the larger nanoparticles within the Gaussian distribution can be heated more efficiently than smaller nanoparticles because they have a longer LSPR wavelength. The LSPR of the redder particles blue-shifts, while the bluer particles are unchanged, which leads to the blue shift and bandwidth narrowing of the overall LSPR band.

In the case of the resonant condition, however, all of the nanoparticles can be heated efficiently; therefore, the bandwidth broadening after laser exposure cannot be explained by the argument above. When the laser is focused on the sample, the laser intensity shows a Gaussian profile; therefore, the nanoparticles are heated inhomogeneously. Because the LSPR of

the nanoparticles is monitored by white light having a spot size similar to the laser spot size, the resulting spectra is the average of all of the nanoparticles with different amounts of shape deformation, which leads to the broadened overall LSPR band.

IV. Conclusion

The laser-induced LSPR change was monitored for NSL-fabricated bare silver nanoparticles and silver nanoparticles coated with 0.4 and 1.0 nm of Al_2O_3. A blue shift of the LSPR band was observed after laser exposure, and this blue shift was explained by the rounded tips of the nanoparticles induced by laser heating. The blue shift of the LSPR became larger as the laser pulse energy increased both for the resonant and off-resonant conditions. The resonant condition showed a larger blue shift than the off-resonant condition for the same laser pulse energy because the laser energy can be more efficiently absorbed by the nanoparticles if the laser is resonant with the LSPR. The LSPR change after laser exposure was reduced when the silver nanoparticles were coated with ALD Al_2O_3 layers, and coating with 1.0 nm of Al_2O_3 showed enhanced protection compared with that for nanoparticles coated with 0.4 nm of Al_2O_3. The decreased LSPR shift of the nanoparticles coated with Al_2O_3 compared to that of the bare nanoparticle was explained by an increased surface melting temperature, which results from the decreased mean square displacement of the atoms located on the nanoparticle surface. The LSPR bandwidth was broadened for the resonant condition, while a slight narrowing of the LSPR band was observed for the off-resonant condition. The bandwidth broadening for the resonant condition was explained by inhomogeneous sample heating caused by the Gaussian beam intensity profile. In the case of the off-resonant condition, more efficient heating of the redder nanoparticles within the sample led to bandwidth narrowing.

It is demonstrated that the ALD Al_2O_3 layers provide enhanced stability of silver nanoparticles against femtosecond laser exposure, and therefore, the Al_2O_3-coated nanoparticles can serve as a stable platform for surface-enhanced laser spectroscopy, including nonlinear spectroscopy. In the case of silver nanoparticles coated with 1.0 nm of Al_2O_3, 10 times higher laser pulse intensity can be used compared to that when the bare nanoparticles are used as substrates. However, there is a trade off because the local field enhancement by the nanoparticles drops quickly as the distance from the nanoparticle surface increases.[74] Therefore, the thickness of the Al_2O_3 layer should be carefully designed for the application as a substrate for laser spectroscopy. The work presented in this paper will provide criteria for selection of nanoparticle substrate and laser pulse intensity for various femtosecond laser spectroscopies.

Future work will be focused on testing the laser power stability of preannealed nanoparticles and such particles with Al_2O_3 layers. The preannealing can be performed by moderate thermal heating[49] or incubation in organic solvents such as methanol,[58] and it is expected to reduce the sensitivity of the nanoparticle LSPR to laser exposure.

Acknowledgment. The authors gratefully acknowledge support from the Air Force Office of Scientific Research (MURI Program Grant F49620-02-1-0381), the DTRA JSTO Program (Grant FA9550-06-1-0558), the National Science Foundation (EEC-0647560, CHE-0414554, DMR-0520513, BES-0507036), and the U.S. Department of Energy (DE-FG02-03ER15457).

References and Notes

(1) Bohren, C. F.; Huffman, D. R. *Absorption and Scattering of Light by Small Particles*; Wiley-VCH: Weinheim, Germany 2004.
(2) Haynes, C. L.; Van Duyne, R. P. *J. Phys. Chem. B* **2001**, *105*, 5599.
(3) Chan, G. H.; Zhao, J.; Hicks, E. M.; Schatz, G. C.; Van Duyne, R. P. *Nano Lett.* **2007**, *7*, 1947.
(4) Jensen, T. R.; Duval, M. L.; Kelly, K. L.; Lazarides, A. A.; Schatz, G. C.; Van Duyne, R. P. *J. Phys. Chem. B* **1999**, *103*, 9846.
(5) Kelly, K. L.; Coronado, E.; Zhao, L.; Schatz, G. C. *J. Phys. Chem. B* **2003**, *107*, 668.
(6) Haes, A. J.; Van Duyne, R. P. *J. Am. Chem. Soc.* **2002**, *124*, 10596.
(7) Zhao, J.; Das, A.; Zhang, X.; Schatz, G. C.; Sligar, S. G.; Van Duyne, R. P. *J. Am. Chem. Soc.* **2006**, *128*, 11004.
(8) Henglein, A.; Meisel, D. *J. Phys. Chem. B* **1998**, *102*, 8364.
(9) Elghanian, R.; Storhoff, J. J.; Mucic, R. C.; Letsinger, R. L.; Mirkin, C. A. *Science* **1997**, *277*, 1078.
(10) Dirix, Y.; Bastiaansen, C.; Caseri, W.; Smith, P. *Adv. Mater.* **1999**, *11*, 223.
(11) Ebbesen, T. W.; Lezec, H. J.; Ghaemi, H. F.; Thio, T.; Wolff, P. A. *Nature* **1998**, *391*, 667.
(12) Knoll, W. *Annu. Rev. Phys. Chem.* **1998**, *49*, 569.
(13) Quinten, M.; Leitner, A.; Krenn, J. R.; Aussenegg, F. R. *Opt. Lett.* **1998**, *23*, 1331.
(14) Brongersma, M. L.; Hartman, J. W.; Atwater, H. A. *Phys. Rev. B* **2000**, *62*, R16356.
(15) Egusa, S.; Liau, Y. H.; Scherer, N. F. *Appl. Phys. Lett.* **2004**, *84*, 1257.
(16) Freeman, R. G.; Grabar, K. C.; Allison, K. J.; Bright, R. M.; Davis, J. A.; Guthrie, A. P.; Hommer, M. B.; Jackson, M. A.; Smith, P. C.; Walter, D. G.; Natan, M. J. *Science* **1995**, *267*, 1629.
(17) McFarland, A. D.; Young, M. A.; Dieringer, J. A.; Van Duyne, R. P. *J. Phys. Chem. B* **2005**, *109*, 11279.
(18) Kahl, M.; Voges, E.; Kostrewa, S.; Viets, C.; Hill, W. *Sens. Actuators, B* **1998**, *51*, 285.
(19) Jeanmaire, D. L.; Van Duyne, R. P. *J. Electroanal. Chem.* **1977**, *84*, 1.
(20) Moskovits, M. *Rev. Mod. Phys.* **1985**, *57*, 783.
(21) Nie, S.; Emory, S. R. *Science* **1997**, *275*, 1102.
(22) Clark, H. A.; Campagnola, P. J.; Wuskell, J. P.; Lewis, A.; Loew, L. M. *J. Am. Chem. Soc.* **2000**, *122*, 10234.
(23) Chen, K.; Durak, C.; Heflin, J. R.; Robinson, H. D. *Nano Lett.* **2007**, *7*, 254.
(24) Eisenthal, K. B. *Chem. Rev.* **2006**, *106*, 1462.
(25) Baldelli, S.; Eppler, A. S.; Anderson, E.; Shen, Y. R.; Somorjai, G. A. *J. Chem. Phys.* **2000**, *113*, 5432.
(26) Kweskin, S. J.; Rioux, R. M.; Habas, S. E.; Komvopoulos, K.; Yang, P.; Somorjai, G. A. *J. Phys. Chem. B* **2006**, *110*, 15920.
(27) Kawai, T.; Neivandt, D. J.; Davies, P. B. *J. Am. Chem. Soc.* **2000**, *122*, 12031.
(28) Liang, E. J.; Weippert, A.; Funk, J.-M.; Materny, A.; Kiefer, W. *Chem. Phys. Lett.* **1994**, *227*, 115.
(29) Koo, T.-W.; Chan, S.; Berlin, A. A. *Opt. Lett.* **2005**, *30*, 1024.
(30) Ichimura, T.; Hayazawa, N.; Hashimoto, M.; Inouye, Y.; Kawata, S. *J. Raman Spectrosc.* **2003**, *34*, 651.
(31) Hayazawa, N.; Ichimura, T.; Hashimoto, M.; Inouye, Y.; Kawata, S. *J. Appl. Phys.* **2004**, *95*, 2676.
(32) Hulteen, J. C.; Young, M. A.; Van Duyne, R. P. *Langmuir* **2006**, *22*, 10354.
(33) Wenseleers, W.; Stellacci, F.; Meyer-Friedrichsen, T.; Mangel, T.; Bauer, C. A.; Pond, S. J. K.; Marder, S. R.; Perry, J. W. *J. Phys. Chem. B* **2002**, *106*, 6853.
(34) Link, S.; El-Sayed, M. A. *Annu. Rev. Phys. Chem.* **2003**, *54*, 331.
(35) Hartland, G. V. *J. Chem. Phys.* **2002**, *116*, 8048.
(36) Hodak, J. H.; Henglein, A.; Hartland, G. V. *J. Phys. Chem. B* **2000**, *104*, 9954.
(37) Hu, M.; Wang, X.; Hartland, G. V.; Mulvaney, P.; Juste, J. P.; Sader, J. E. *J. Am. Chem. Soc.* **2003**, *125*, 14925.
(38) Huang, W.; Qian, W.; El-Sayed, M. A. *Nano Lett.* **2004**, *4*, 1741.
(39) Huang, W.; Qian, W.; El-Sayed, M. A. *J. Phys. Chem. B* **2005**, *109*, 18881.
(40) Habenicht, A.; Olapinski, M.; Burmeister, F.; Leiderer, P.; Boneberg, J. *Science* **2005**, *309*, 2043.
(41) Kaempfe, M.; Rainer, T.; Berg, K.-J.; Seifert, G.; Graener, H. *Appl. Phys. Lett.* **1999**, *74*, 1200.
(42) Miranda, M. H. G.; Falcão-Filho, E. L.; Rodrigues, J. J.; de Araújo, C. B.; Acioli, L. H. *Phys. Rev. B* **2004**, *70*, 161401.
(43) Link, S.; Burda, C.; Mohamed, M. B.; Nikoobakht, B.; El-Sayed, M. A. *J. Phys. Chem. A* **1999**, *103*, 1165.
(44) Shi, F. G. *J. Mater. Res.* **1994**, *9*, 1307.
(45) Buffat, P.; Borel, J.-P. *Phys. Rev. A* **1976**, *13*, 2287.
(46) Dick, K.; Dhanasekaran, T.; Zhang, Z.; Meisel, D. *J. Am. Chem. Soc.* **2002**, *124*, 2312.
(47) Huang, W.; Qian, W.; El-Sayed, M. A. *J. Am. Chem. Soc.* **2006**, *128*, 13330.

(48) Huang, W.; Qian, W.; El-Sayed, M. A. *J. Appl. Phys.* **2005**, *98*, 114301.

(49) Whitney, A. V.; Elam, J. W.; Stair, P. C.; Van Duyne, R. P. *J. Phys. Chem. C* **2007**, *111*, 16827.

(50) Bañares, M. A. *Catal. Today* **2005**, *100*, 71.

(51) Hulteen, J. C.; Van Duyne, R. P. *J. Vac. Sci. Technol., A* **1995**, *13*, 1553.

(52) Elam, J. W.; Groner, M. D.; George, S. M. *Rev. Sci. Instrum.* **2002**, *73*, 2981.

(53) Ott, A. W.; Klaus, J. W.; Johnson, J. M.; George, S. M. *Thin Solid Films* **1997**, *292*, 135.

(54) Groner, M. D.; Fabreguette, F. H.; Elam, J. W.; George, S. M. *Chem. Mater.* **2004**, *16*, 639.

(55) Whitney, A. V.; Elam, J. W.; Zou, S.; Zinovev, A. V.; Stair, P. C.; Schatz, G. C.; Van Duyne, R. P. *J. Phys. Chem. B* **2005**, *109*, 20522.

(56) Moran, A. M.; Sung, J.; Hicks, E. M.; Van Duyne, R. P.; Spears, K. G. *J. Phys. Chem. B* **2005**, *109*, 4501.

(57) Marin, T. W.; Homoelle, B. J.; Spears, K. G.; Hupp, J. T.; Spreer, L. O. *J. Phys. Chem. A* **2002**, *106*, 1131.

(58) Malinsky, M. D.; Kelly, K. L.; Schatz, G. C.; Van Duyne, R. P. *J. Am. Chem. Soc.* **2001**, *123*, 1471.

(59) Jensen, T. R.; Malinsky, M. D.; Haynes, C. L.; Van Duyne, R. P. *J. Phys. Chem. B* **2000**, *104*, 10549.

(60) Zhang, X.; Hicks, E. M.; Zhao, J.; Schatz, G. C.; Van Duyne, R. P. *Nano Lett.* **2005**, *5*, 1503.

(61) Tabor, C.; Qian, W.; El-Sayed, M. A. *J. Phys. Chem. C* **2007**, *111*, 8934.

(62) Del Fatti, N.; Voisin, C.; Achermann, M.; Tzortzakis, S.; Christofilos, D.; Vallée, F. *Phys. Rev. B* **2000**, *61*, 16956.

(63) Voisin, C.; Christofilos, D.; Del Fatti, N.; Vallée, F.; Prével, B.; Cottancin, E.; Lermé, J.; Pellarin, M.; Broyer, M. *Phys. Rev. Lett.* **2000**, *85*, 2200.

(64) Hodak, J. H.; Martini, I.; Hartland, G. V. *J. Phys. Chem. B* **1998**, *102*, 6958.

(65) Arbouet, A.; Voisin, C.; Christofilos, D.; Langot, P.; Del Fatti, N.; Vallée, F.; Lermé, J.; Celep, G.; Cottancin, E.; Gaudry, M.; Pellarin, M.; Broyer, M.; Maillard, M.; Pileni, M. P.; Treguer, M. *Phys. Rev. Lett.* **2003**, *90*, 177401.

(66) Link, S.; Burda, C.; Nikoobakht, B.; El-Sayed, M. A. *Chem. Phys. Lett.* **1999**, *315*, 12.

(67) Link, S.; Hathcock, D. J.; Nikoobakht, B.; El-Sayed, M. A. *Adv. Meter.* **2003**, *15*, 393.

(68) Haes, A. J.; Zou, S.; Schatz, G. C.; Van Duyne, R. P. *J. Phys. Chem. B* **2004**, *108*, 109.

(69) *CRC Handbook of Chemistry and Physics*, 82nd ed.; CRC Press: Boca Raton, FL, 2001.

(70) Link, S.; El-Sayed, M. A. *J. Phys. Chem. B* **1999**, *103*, 8410.

(71) Hulteen, J. C.; Treichel, D. A.; Smith, M. T.; Duval, M. L.; Jensen, T. R.; Van Duyne, R. P. *J. Phys. Chem. B* **1999**, *103*, 3854.

(72) Westcott, S. L.; Averitt, R. D.; Wolfgang, J. A.; Nordlander, P.; Halas, N. J. *J. Phys. Chem. B* **2001**, *105*, 9913.

(73) Lindemann, F. A. *Phys. Z* **1910**, *11*, 609.

(74) Dieringer, J. A.; McFarland, A. D.; Shah, N. C.; Stuart, D. A.; Whitney, A. V.; Yonzon, C. R.; Young, M. A.; Zhang, X.; Van Duyne, R. P. *Faraday Discuss.* **2006**, *132*, 9.